7th Australasian Hydraulics and
Fluid Mechanics Conference,
Brisbane, 18-22 August, 1980

Topographic Forcing in Nonlinear and Linear Barotropic Models

J.S. FREDERIKSEN and B.L. SAWFORD
Senior Research Scientists, Division of Atmospheric Physics, CSIRO, Victoria

SUMMARY The role of topography in forcing the stationary eddy flow field of the atmosphere is studied using the spherical equivalent barotropic model. The importance of nonlinear interactions is probed by comparing nonlinear statistical mechanical equilibrium solutions with linear steady state solutions.

1 INTRODUCTION

Many studies have been made of the effect of orography and diabatic heating in forcing the stationary planetary-scale flow field of the atmosphere. These range from a linearized treatment of a barotropic model incorporating topographic forcing only (the earliest being that by Charney and Eliassen, 1949), through simple baroclinic models forced by heating, to numerical simulation in multilevel global circulation models, which include both topographic and thermal forcing. The most recent full scale model study is that of Manabe and Terpstra (1974), who also review the intervening literature.

While full scale numerical studies have added to our understanding, such results are difficult to generalize and may be subject to uncertainty due to doubts concerning the adequacy of the resolution achieved. Consequently, further theoretical studies using simplified models have since been made (for example, Grose and Hoskins (1979), Egger (1976)) in order to provide further insight into the dynamical effects of orography in particular. Although these semi-analytic models are much more transparent than the large numerical models, they are subject to a number of simplifying assumptions, the effect of which is largely unknown. In particular, the linearity assumption, in which interactions among stationary waves, and between stationary and transient disturbances are neglected, appears to be universal.

In this article, a topographically forced inviscid barotropic model in spherical geometry is used to compare fully nonlinear and linearized solutions for the stationary waves. Although differing in minor detail, the linear solutions we present are very similar to those of Grose and Hoskins (1979), and the main interest here centres on the nonlinear solutions, which we obtain using the methods of statistical mechanics. Such methods are well known in the theory of two-dimensional turbulence (Kraichnan, 1975), but have only recently been applied directly to flows of relevance to the atmosphere by Frederiksen and Sawford (1980a). In that study, statistical mechanical solutions were used to explain some unusual features which occur in the evolution of unforced inviscid barotropic models, and which also occur in multilevel models incorporating both diabatic heating and viscosity.

Thus, although we emphasize that the present barotropic study neglects diabatic heating and baroclinic effects and as such, cannot be expected to reproduce accurately observed stationary global flow fields, we hope to gain from these statistical mechanical solutions valuable insights into the consequences of nonlinear interactions and so improve, at least qualitatively, our understanding of the effects of orographic forcing.

2 THEORY

2.1 Model Details

Taking a_o (earth's radius) and Ω^{-1} (earth's angular velocity)$^{-1}$ as length and time scales, the non-dimensional equations defining our spherical equivalent barotropic model are

$$\partial\nabla^2\psi/\partial t + J(\psi, \nabla^2\psi + 2\mu + h) = 0 \qquad (1)$$

where

$$h = 2\,\mu g\, AH/RT \qquad (2)$$

and

$$J(f,g) = \frac{\partial f}{\partial \lambda}\frac{\partial g}{\partial \mu} - \frac{\partial f}{\partial \mu}\frac{\partial g}{\partial \lambda} \qquad (3)$$

Here, ψ is the streamfunction, μ = sin (latitude), λ = longitude, t is the time, H is the height of the topography, R is the gas constant, T the horizontally averaged global surface temperature, g the acceleration due to gravity and A is the value of the vertical profile factor at 1000 mb (see, for example, Holton (1972), p.129). We take A = 0.8, R = 287 J kg^{-1} K^{-1} and T = 273 K, in order to match the linear solutions to (1) with those of Grose and Hoskins (1979) who use the corresponding free surface equations with a mean free surface height of 10 km.

Solutions to (1) are obtained in spectral form by expanding both the streamfunction and the forcing function, $\hat{h} = 2\mu + h$, in spherical harmonics:

$$\psi = \sum_{m=-J}^{J} \sum_{n=|m|}^{|m|+J} \psi_{mn}\, P_n^m(\mu)\, e^{im\lambda} \qquad (4)$$

and

$$\hat{h} = \sum_{m=-J}^{J} \sum_{n=|m|}^{|m|+J} \hat{h}_{mn}\, P_n^m(\mu)\, e^{im\lambda} \qquad (5)$$

The functions $P_n^m(\mu)$ are normalized associated Legendre functions, ψ_{mn} and $\hat{h}_{mn}$ are spectral amplitudes, m is the zonal wavenumber, n the total wavenumber, and J the rhomboidal truncation wavenumber.

2.2 Equilibrium Solutions

We present the equilibrium results without derivation. Details of the analysis are given in Frederiksen and Sawford (1980a,b) and in references

contained therein. An essential property of the barotropic equation is that the total energy E and potential enstrophy F, where

$$E = \tfrac{1}{4} \sum_{m=-J}^{J} \sum_{n=|m|}^{|m|+J} n(n+1)\ |\psi_{mn}|^2 \qquad (6)$$

and

$$F = \tfrac{1}{4} \sum_{m=-J}^{J} \sum_{n=|m|}^{|m|+J} |\ n(n+1)\ \psi_{mn} - \hat{h}_{mn}|^2, \qquad (7)$$

are invariant.

Now, the equilibrium solutions consist of ensemble averages (over a large number of realizations of the system, all with the same E and F) which are equivalent to long-time averages over a single realization. For the forced system here, the expectations of the spectral coefficients are non-zero,

$$\langle\psi_{mn}\rangle = \beta\ \hat{h}_{mn}/[\alpha + \beta\ n(n+1)]. \qquad (8)$$

The expectation for the energy, E_{mn}, in the mn mode is

$$E_{mn} = \tfrac{1}{2}/[\alpha + \beta\ n(n+1)] + \tfrac{1}{4}\ n(n+1)\,|\langle\psi_{mn}\rangle|^2. \qquad (9)$$

The parameters α, β are determined by equating the expectations for the total energy and potential enstrophy to the invariant values E and F determined by the initial conditions.

Since the ensemble averages are equivalent to long-time averages, (8) clearly represents the stationary part of the streamfunction field. While the expectation of the transient part of the streamfunction is zero, the energy of the transient field is not. Thus we see that the energy expectation (9) consists of two parts. The second term on the right clearly represents the energy of the stationary flow, while the first term represents the energy of the transient flow.

The parameter β is generally positive (Salmon et al., 1976) provided the resolution is not too coarse (that is, the truncation wavenumber J is not too small), and since $\alpha+\beta n(n+1)$ is required to be positive (the transient energy must be positive), we see from (8) that the streamfunction is positively correlated with the topographic field at all scales.

In order to realistically model the zonal flow (which in the atmosphere is largely forced by diabatic heating and baroclinic effects), we introduce the heuristic device of an effective zonal 'thermal mountain'. That is, we adjust the zonal forcing coefficients to reproduce a specified zonal flow. Full details of the procedure are given in Frederiksen and Sawford (1980b). The nett result is that the equilibrium solutions are used only to calculate the eddy part of the stationary flow field, and depend not only on E and F, but also on the given climatological zonal streamfunction coefficients. In practice, qualitative features of the eddy field are quite insensitive to the details of the model, and our results do not depend strongly on the thermal mountain artifice.

2.3 Linear Solutions

To allow comparison with the results of Grose and Hoskins (1979), we include a linear drag term and a biharmonic diffusion term in (1), which after linearizing the eddy terms, becomes at steady state

$$J(\overline{\psi},\nabla^2\psi'+h) + J(\psi',\nabla^2\overline{\psi}+2\mu) + \kappa\nabla^2\psi' + \kappa'\nabla^6\psi' = 0. \qquad (10)$$

Here, $\overline{\psi}$ is the fixed zonal flow streamfunction, ψ' is the stationary eddy streamfunction, and κ and κ' are drag and diffusion coefficients respectively.

To clarify the comparison with the nonlinear solutions, we present two special cases of the solution to (10). The complete solution involves a set of simultaneous linear equations, and is conveniently but not very transparently handled numerically. Full details are given in Frederiksen and Sawford (1980b). First, we ignore drag and diffusion, and consider the special case when the zonal flow is solid-body rotation,

$$\overline{\psi} = \overline{\psi_{01}}\ P_1^0(\mu) = -\gamma\mu \text{ where } \gamma = -\sqrt{3/2}\ \overline{\psi_{01}} > 0. \qquad (11)$$

Then,

$$\psi'_{mn} = \gamma\ \hat{h}_{mn}/[-2(\gamma+1) + \gamma n(n+1)] \qquad (12)$$

Second, for the same zonal flow, but with drag and diffusion included,

$$\psi'_{mn} = \gamma\ \hat{h}_{mn}\ r\ e^{i\theta}, \qquad (13)$$

where

$$r^{-1} = \{[\gamma n(n+1) - 2(\gamma+1)]^2 + [\kappa n(n+1) + \kappa'\ n^3(n+1)^3]^2/m^2\}^{1/2} \qquad (14)$$

and

$$\theta = \arccos\{[\gamma n(n+1) - 2(\gamma+1)]r\}. \qquad (15)$$

3 COMPARISON OF LINEAR AND NONLINEAR SOLUTIONS

3.1 Superrotation Zonal Flow Without Drag or Friction

In this case, the linear solution (12) has the same form as the nonlinear equilibrium solution (8), with γ replacing β and $-2(\gamma+1)$ replacing α. However, whereas (8) implies a positive correlation at all scales between the topography and the streamfunction amplitudes, for the linear case, long waves for which $-2(\gamma+1) + \gamma n(n+1) < 0$ are negatively correlated with the topography. Furthermore, the linear solutions exhibit resonance (or near-resonance, depending on the strength of the zonal superrotation) for values of n at or near n_r, where $n_r\ (n_r+1) = 2(\gamma+1)/\gamma$. Thus, in these linear solutions, the effect of topographic forcing on scales with total wavenumber near n_r and zonal wavenumbers up to $m \approx n_r$ is enhanced.

In contrast, the nonlinear solutions show no resonance phenomenon. The stationary streamfunction amplitudes in (8) are proportional to the topographic amplitudes weighted by the equilibrium transient energy. For the usual case of a red energy spectrum, the streamfunction field is thus merely a low-pass filtered version of the topographic field.

These contrasting features of the two solutions show up clearly in Fig. 1, which shows the eddy component of the 500 mb geopotential height fields (superimposed on a mean value of 5400 m) forced by a single circular mountain 2500 m high centred at 30°N and 180°W, with a diameter of 45° latitude. The zonal flow

$$\overline{\psi}_{01} = -0.02645 \quad \text{or} \quad \gamma = 0.03239 \qquad (16)$$

is the solid-body rotation used by Grose and Hoskins (1979), and corresponds to a maximum zonal velocity at the equator of 15.1 ms^{-1}, and a resonant total wavenumber, 7.5. In accord with the remarks above,

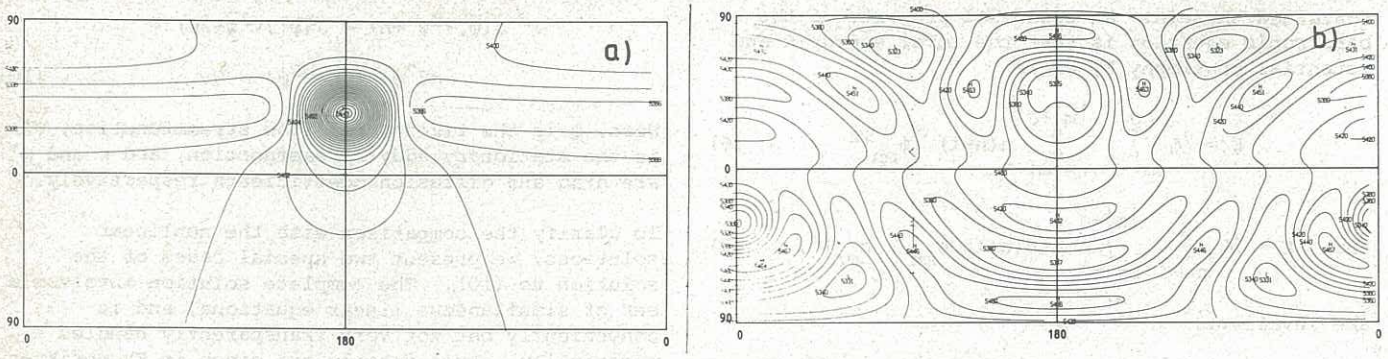

Figure 1 Nonlinear (a) and linear (b) 500 mb eddy geopotential height fields forced by the superrotation zonal flow, (18), over a circular mountain.

note that the nonlinear eddy field in Fig. 1(a) closely reflects the topography of the circular mountain, and features a high over the mountain with no small scale structure upstream or downstream. In contrast, the linear eddy field in Fig. 1(b) is anticorrelated with topography at large scales, so there is a low over the mountain. The resonant emphasis of smaller scales results in a great deal of structure in the rest of the field. Particularly striking is the wavetrain which propagates into the Southern Hemisphere and then back to the upstream side of the mountain. Both the nonlinear and linear fields are symmetrical in longitude.

3.2 Drag and Friction in the Linear Model

Comparing (13) with (12), we see that the effects of drag and friction are two-fold. First, the amplitude of ψ'_{mn} is reduced by a factor $r|\gamma n(n+1) - 2(\gamma+1)|$. This reduction is most dramatic if (12) is a resonant solution, and is also greater for small values of the zonal wavenumber. Second, the term $e^{i\theta}$ in (13) rotates the appropriate streamfunction component. For example, the zonal harmonic $e^{im\lambda}$ undergoes a rotation of θ/m relative to the case with no drag. Thus the degree of rotation also decreases with increasing m.

To quantify these effects, we consider the superrotation zonal flow (16) with non-dimensional drag and diffusion coefficients $\kappa = 0.011507$ and $\kappa' = 1.946 \times 10^{-7}$, which have been chosen to correspond closely with those of Grose and Hoskins (1979). Without drag or diffusion, the solutions are near-resonant with large ψ'_{mn} for n near $n_r = 7.5$. With drag and diffusion, the P_7^1 mode amplitude is reduced by a factor of 3, the P_7^2 mode by only a third and the P_7^7 mode suffers hardly any reduction. Similarly, the rotation relative to the no-drag case varies from about 70° for the P_1^1 mode to about 20° for the P_7^7 mode.

Thus, although the inclusion of drag prevents the occurrence of mathematical singularities in the linear solutions, and results in significant changes in the perturbation streamfunction, the quasi-resonant behaviour and hence the sensitivity to changes in the zonal flow, remains. Scales near the resonant wavenumber are still emphasized, and individual waves are phase-shifted relative to the corresponding topographic component. Details of the comparison in Section 3.1 are essentially unaltered by the effects of drag and diffusion. Thus, the linear eddy geopotential height field shown in Fig. 3(c) of Grose and Hoskins (1979) is basically anticorrelated with topography at large scales, with a weak upslope anticyclone and a stronger downslope cyclone, the latter being the dominant feature over the mountain. The wavetrain, while still prominent downstream, is attenuated by drag and is virtually absent upstream of the mountain. Drag thus destroys the symmetry of the eddy field.

3.3 Realistic Zonal Flow

Finally, we consider the general case with realistic shear in the zonal flow. For the linear model, we again draw on the results of Grose and Hoskins (1979). The main feature noted by those authors is that equatorial easterlies in the zonal flow prevent propagation of the wavetrain through the tropics into the Southern Hemisphere. In other respects, there is close similarity to superrotation results. Large scales are still essentially anticorrelated with topography; the downstream wavetrain, although confined to the Northern Hemisphere, is still prominent, and the scale of the wavetrain is strongly dependent on the strength of the zonal flow.

The form (8) of the nonlinear solutions is unchanged by variations in the zonal flow, and the resulting eddy field remains qualitatively similar to Fig. 1(a). Thus, even for quite general zonal flows, and with the inclusion of drag in the linear model, the essential differences between the nonlinear and linear solutions are encapsulated in the comparison between the simplified cases of Section 3.1.

4 CLIMATOLOGICAL ZONAL FLOWS WITH GLOBAL TOPOGRAPHY

Here we examine the nonlinear equilibrium solutions and the linear solutions corresponding to observed December to February mean zonal flows over global topography. We consider three levels, 850 mb, 500 mb and 300 mb, for which mean zonal flows are tabulated in Newell et al. (1969). We are concerned only with making qualitative comparisons with observed stationary fields.

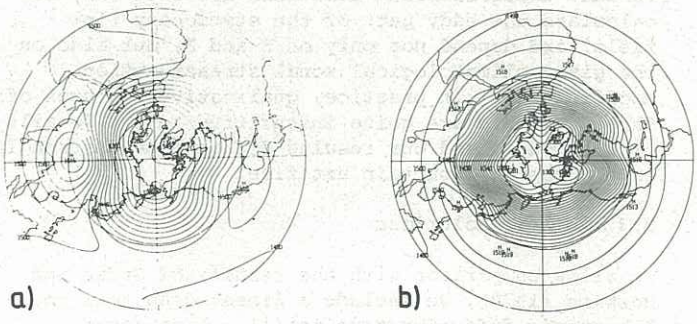

Figure 2 Nonlinear (a) and linear (b) NH 850 mb geopotential height forced by Dec.-Feb. 850 mb mean zonal flow over global topography.

For the statistical mechanical solutions with the 850 mb mean zonal flow, we take typical values for E and F from an observed instantaneous IGY global streamfunction (see Fig. 1 of Puri and Bourke, 1974). As expected from the form of (8) and the discussion in Section 3, the eddy geopotential height field is essentially a filtered version of the topography, with highs over the mountain ranges of the Himalayas, Rockies and Greenland and lows in the North Atlantic and Pacific Oceans. Similarly, in the Southern Hemisphere, there is a principle high over the Antarctic plateau, subsidiary highs over the Andes and southern Africa, and a low extending from the Ross to Weddell Seas. Fig. 2(a) shows the equilibrium values for the Northern Hemisphere 850 mb geopotential height field (eddy plus zonal, superimposed on a mean value of 1450 m). For comparison, Fig. 2(b) shows the corresponding linear field. Comparing them with the observed field in Chart 1.4 of Crutcher and Meserve (1970), we see that the nonlinear field has the basic observed features of the Aleutian low, ridging over the Rockies, a trough near Hudson Bay and a high over Greenland; further, it has a low slightly north of Norway and shows the presence of the Siberian high. In constrast, the linear solution is a poor representation of the basic features; there is no Aleutian low and no ridging over the Rockies, but instead there are misplaced lows over Greenland and northern Siberia and ridging on the east American coast.

As in Section 3, the nonlinear eddy fields are qualitatively insensitive to variation in the mean zonal field, so that the 500 mb and 300 mb eddy geopotential height fields essentially mimic the features of the 850 mb field. Consequently, the observed westward tilt with increasing altitude is not reproduced, apparently because of the absence of drag and baroclinic effects in the model. We also note that for the linear theory, for which the 500 mb streamfunction is shown in Fig. 7 of Grose and Hoskins (1979), the comparison with observation is also quite poor. However, those authors note (see their Fig. 6) that the 300 mb linear field is very realistic. The reason for this appears to be that the stronger 300 mb zonal flow forces resonance closer to the prominent m = 3 topographic scales, which thus dominate the 300 mb eddy geopotential height field. It should be noted, however, that this agreement depends to some extent at least on the drag used. As the drag is decreased to zero, the low over northern Siberia rotates westward by about 80°.

5 CONCLUSIONS

The considerable differences between the two types of solution arise largely from the fact that the linear solutions are resonant or near resonant while the nonlinear solutions are not. Thus the nonlinear eddy fields are relatively insensitive to variations over the parameter range of interest, but the linear fields depend strongly on the strength of the zonal flow. Further, while the nonlinear flow is positively correlated with topography at all scales, the linear fields are anti-correlated at large scales. Drag and diffusion, although resulting in considerable changes to the linear solutions, do not alter these conclusions.

Results obtained using climatological zonal flows with real topography show that nonlinear effects are most important at low altitudes, and that the linearized solution is most realistic at high levels, where the zonal flow is large, and the assumption of a small perturbation eddy field is more nearly satisfied.

6 REFERENCES

CHARNEY, J.G. and ELIASSEN, A. (1949). A numerical method for predicting the perturbations of the middle latitude westerlies. Tellus, Vol. 1, pp 38-54.

CRUTCHER, H.L. and MESERVE, J.M. (1970). Selected level heights, temperature, and dew points for the Northern Hemisphere. NAVAIR-50-1C-52. [Available from Naval Weather Service Command, Washington Navy Yard, Washington, D.C.].

EGGER, J. (1976). The linear response of a hemispheric two level primitive equation model to forcing by topography. Mon.Wea.Rev., Vol. 104, pp 351-364.

FREDERIKSEN, J.S. and SAWFORD, B.L. (1980a). Statistical dynamics of two-dimensional inviscid flow on a sphere. J.Atmos.Sci. (In press).

FREDERIKSEN, J.S. and SAWFORD, B.L. (1980b). Topographic waves in nonlinear and linear spherical barotropic models. Submitted to J.Atmos.Sci.

GROSE, W.L. and HOSKINS, B.J. (1979). On the influence of orography on large-scale atmospheric flow. J.Atmos.Sci., Vol. 36, pp 223-234.

HOLTON, J.R. (1972). An introduction to dynamic meteorology. New York, Academic Press.

KRAICHNAN, R.H. (1975). Statistical dynamics of two-dimensional flow. J.Fluid Mech., Vol. 67, pp 155-175.

MANABE, S. and TERPSTRA, T.B. (1974). The effects of mountains on the general circulation of the atmosphere as identified by numerical experiments. J.Atmos.Sci., Vol. 31, pp 3-42.

NEWELL, R.E., VINCENT, T.G., FERRUZA, T. and KIDSON, J.W. (1969). The energy balance of the global atmosphere, pp 42-90 in The global circulation of the atmosphere. (G.A. CORBY, Ed.). Roy.Meteor.Soc.

PURI, K. and BOURKE, W. (1974). Implications of horizontal resolution in spectral model integrations. Mon.Wea.Rev., Vol. 102, pp 333-347.

SALMON, R., HOLLOWAY, G. and HENDERSHOTT, M.C. (1976). The equilibrium statistical mechanics of simple quasi-geostrophic models. J.Fluid Mech., Vol. 75, pp 691-703.